Spatiotemporal Evolution Analysis of Construction Land Expansion in Wuhan East Lake High-tech Development Zone Based on Remote Sensing

Zunran Wang

School of Public Administration, China University of Geosciences, Wuhan, China

1037568096@cug.edu.cn

Abstract. Focusing on Wuhan's East Lake High-tech Development Zone, this paper draws upon Landsat imagery and land use records from three years—2005, 2015, and 2025. Land use dynamics were mapped in ArcMap, and the environmental ripple effects of construction land growth were evaluated using the Normalized Difference Vegetation Index (NDVI) alongside Land Surface Temperature (LST). The data show that construction land within the zone expanded from 43.61 km² to 121.72 km² across the two decades, an increase of roughly 179%, with growth fanning out mainly toward the east and south. Cropland steadily gave way to urban uses. A tight spatial coupling emerged among the three datasets. Gains in construction land coincided with thinning vegetation and climbing surface temperatures. Meanwhile, East Lake and its surrounding green belts remained cool and densely vegetated, serving as a critical buffer against the urban heat island and helping sustain regional ecological stability. The results can inform land allocation strategies and territorial spatial planning for the zone.

Keywords: Land use change, NDVI, Land surface temperature, Remote sensing monitoring, East Lake High-tech Development Zone.

1. Introduction

Land use change is perhaps the most direct spatial signature of urbanization. Over the past two decades, China's urban construction land has expanded dramatically. In Wuhan, Tong and Lang tracked sustained construction land growth using remote sensing [1]. Huang et al. showed that GDP growth alone accounts for roughly 68% of the variation in construction land expansion based on a driving force analysis [2]. Construction land expansion supports economic growth, but it also eats into cropland and ecological space while making the urban heat island worse. Tracking these expansion processes and their environmental effects calls for large-scale, multi-temporal spatial data—exactly the kind of work remote sensing is built for.

Thanks to its broad coverage and short revisit times, remote sensing has become the go-to tool for monitoring land use change and eco-environmental conditions. Chang and Li confirmed that 30 m Landsat imagery works well for urban land classification in Wuhan through supervised classification[3]. Su et al. examined how land use changes shape Wuhan's urban heat island using remote sensing inversion [4]. That said, most existing work looks at single indicators at the municipal scale and rarely brings together construction land expansion, vegetation cover change, and surface thermal effects in one analytical framework. Detailed studies of the East Lake High-tech Development Zone—a distinctly fast-growing area—are especially scarce.

The East Lake High-tech Development Zone sits at the heart of China's Optics Valley and has seen rapid industrial clustering and population growth over the past decade. This study uses Landsat imagery from three time points—2005, 2015, and 2025—along with NDVI and LST indicators, to build a systematic picture of how construction land expansion unfolded and what it meant for the environment. Three dimensions are examined: quantitative change, spatial pattern, and ecological effects. The goal is to provide evidence that can inform land resource planning in the study area.

2. Data and Methods

2.1. Study Area Overview

The study area lies in southeastern Wuhan, stretching from 114°17′ to 114°35′ E and 30°22′ to 30°35′ N, covering roughly 518 km² (Fig. 1). It contains East Lake—China's largest urban lake at about 33 km² of water—and has the dual character of an urban development zone and an ecological conservation area. The permanent resident population climbed from about 250,000 in 2005 to roughly 1.2 million in 2025, and the land cover pattern changed profoundly, making the zone a natural laboratory for studying the urban expansion–ecological response relationship.

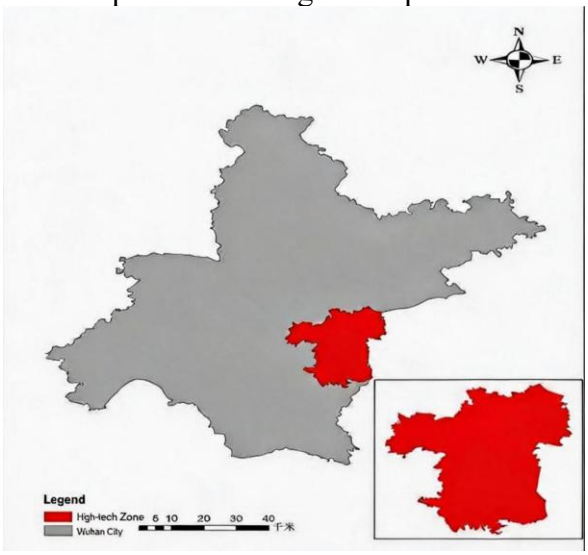
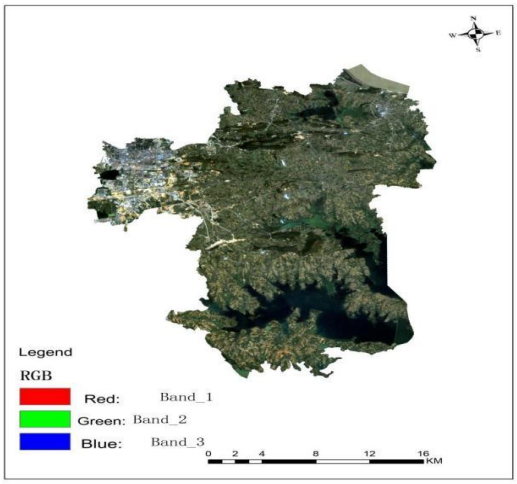


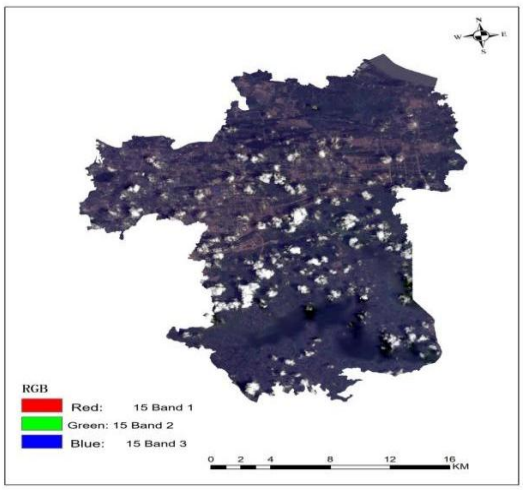
Fig. 1 Location map of Wuhan East Lake High-tech Development Zone (Credit: Original by author).

2.2. Data Sources

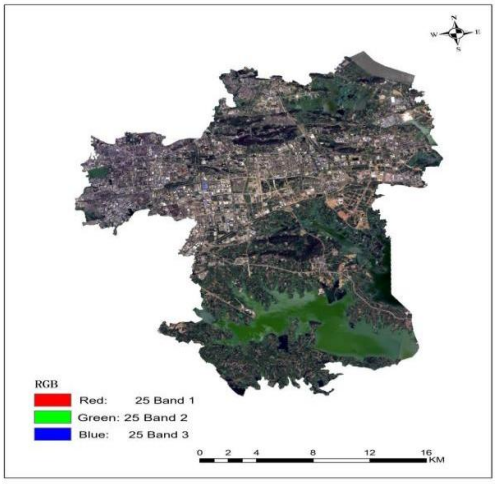
Remote sensing images were all obtained from the USGS EarthExplorer platform, and all images had cloud cover below 5% and favorable atmospheric conditions, ensuring the accuracy of subsequent classification and inversion (Fig. 2) [5-8]. Landsat 5 TM imagery for 2005 (July 2005), and Landsat 8 OLI/TIRS imagery for 2015 (August 2015) and 2025 (August 2025), all with a spatial resolution of 30 m [5-8].



(a)



(b)



(c)

Fig. 2 Landsat false-color composite images for (a) 2005, (b) 2015, (c) 2025 (Credit: Original by author).

Land use was classified into six categories: cropland, forest, grassland, water bodies, bare land, and construction land. Preprocessing steps—coordinate unification to WGS_1984_UTM_Zone_50N, radiometric calibration, and FLAASH atmospheric correction—were carried out in ArcMap 10.8 and ENVI 5.3.

2.3. Research Methods

The methodology had three main parts. First, land use was classified for all three periods using the Maximum Likelihood Classification (MLC) method. To keep the classification statistically sound, at least 60 training samples and 30 independent validation samples were selected for each land cover type. Accuracy was checked with overall accuracy and the Kappa coefficient (results are reported in Section 3). A transition matrix was built to track how much of each land type moved to other categories, and the Single Land Use Dynamic Degree (K) was used to measure the rate of change per unit time.

$$K=\frac{U_b-U_a}{U_a}\times\frac{1}{T}\times 100\% \quad (1)$$

where U_a and U_b are the areas of a given land use type at the start and end of the study period, and T is the period length in years. A positive K means net growth; a negative K means net loss. Two landscape pattern indices—Number of Patches (NP) and Mean Patch Size (MPS)—were also applied to gauge how fragmented the ecological space had become. The impervious surface ratio was simply construction land area divided by total study area. For understanding thermal environment differences, the Local Climate Zone (LCZ) framework developed by Stewart and Oke provided the theoretical foundation [9].

Second, vegetation cover was characterized using the Normalized Difference Vegetation Index (NDVI).

$$\mathrm{NDVI}=\frac{\rho_{NIR}-\rho_R}{\rho_{NIR}+\rho_R} \quad (2)$$

For Landsat 5 TM, Band 3 (Red) and Band 4 (Near Infrared) were used; for Landsat 8 OLI/TIRS, Band 4 (Red) and Band 5 (Near Infrared). NDVI runs from −1 to 1: higher values mean denser, healthier vegetation, and values near zero point to bare soil or impervious surfaces. Following Xu et al., areas with NDVI below 0.2 were treated as high-density built-up land.

Third, land surface temperature (LST) was retrieved using the Radiative Transfer Equation (RTE) approach. The workflow went as follows: radiometric calibration converted image DN values to top-of-atmosphere spectral radiance, and Planck's equation turned that radiance into at-satellite brightness

temperature; the NDVI threshold method estimated land surface emissivity, with values set by fractional vegetation cover zone, and finally, the radiative transfer equation corrected brightness temperature to true LST.

To pin down the quantitative relationships, univariate linear regressions were run with construction land proportion as the predictor and mean NDVI and mean LST as the response variables, using the three-period dataset.

$$L\lambda = Gain \times DN + OffsetL_{\lambda} \tag{3}$$

$$T_b = \frac{K_2}{\ln\left(\frac{K_1}{L_\lambda}+1\right)} \tag{4}$$

where K_1 and K_2 are the calibration constants of the satellite sensor.

$$LST = \frac{T_b}{1+\left(\frac{\lambda \times T_b}{\rho}\right)\times ln(\varepsilon)} \tag{5}$$

where λ is the effective wavelength, and $\rho = h \times c/\sigma$ (h is Planck's constant, c is the speed of light, σ is the Stefan–Boltzmann constant).

3. Results and Discussion

3.1. Characteristics of Construction Land Expansion

Table 1 reports the land use area tallies for the three observation years. Construction land climbed from 43.61 km² (2005) to 121.72 km² (2025), yielding a net addition of 78.11 km² and an overall growth of 179.11%. The pace was not uniform: annual expansion averaged 4.52 km² during 2005–2015 before easing to 3.29 km²/year in the 2015–2025 interval. Yang et al. applied intensity analysis to national central cities and concluded that land use change there has sped up [10]. Even against that backdrop, this zone's construction land grew considerably faster than the Wuhan-wide rate.

Classification quality held up across all three dates: overall accuracy reached 89.2% (2005), 87.8% (2015), and 88.5% (2025); the corresponding Kappa statistics were 0.85, 0.83, and 0.84. Each of these clears the commonly applied accuracy thresholds for land use change detection.

Single land use dynamic degree (K) values reinforce the deceleration pattern. For construction land, K dropped from 10.36% (2005–2015) to 3.71% (2015–2025). Cropland registered −1.38% and −0.77% in the two intervals—still shrinking, but more slowly. Forest, buoyed by conservation programs, saw its K decline from 2.37% to 0.59%, signaling that the growth in forest cover was leveling off.

Table 1. Land use type areas in 2005, 2015 and 2025 (unit: km²).

land type	2005	2015	2025
Farmland	375.55	323.70	298.62
Forest	15.62	19.33	20.47
Grass land	0.13	0.04	0.02
Water area	97.61	100.61	91.68
Bare land	0	0.005	0.03
Construction land	43.61	88.80	121.72

From the perspective of spatial distribution (Fig. 3), in 2005, construction land exhibited a point-like agglomeration pattern centered around Optics Valley Square; by 2015, it extended in a belt-like pattern along major transportation corridors toward the east and south; by 2025, it further expanded toward Zuoling in the east and Tangxun Lake in the south, with a concentric zonal pattern becoming increasingly evident. Huang Duan et al., in their analysis of land use change in the Wuhan metropolitan area, pointed out that transportation infrastructure construction exerts a significant guiding effect on construction land expansion [11].

The transition matrix results show that 76.52 km² of cropland was converted to construction land, accounting for 97.9% of the net increase in construction land. Cropland decreased from 375.55 km² to 298.62 km², while forest, benefiting from ecological conservation policies, increased from 15.62 km² to 20.47 km².

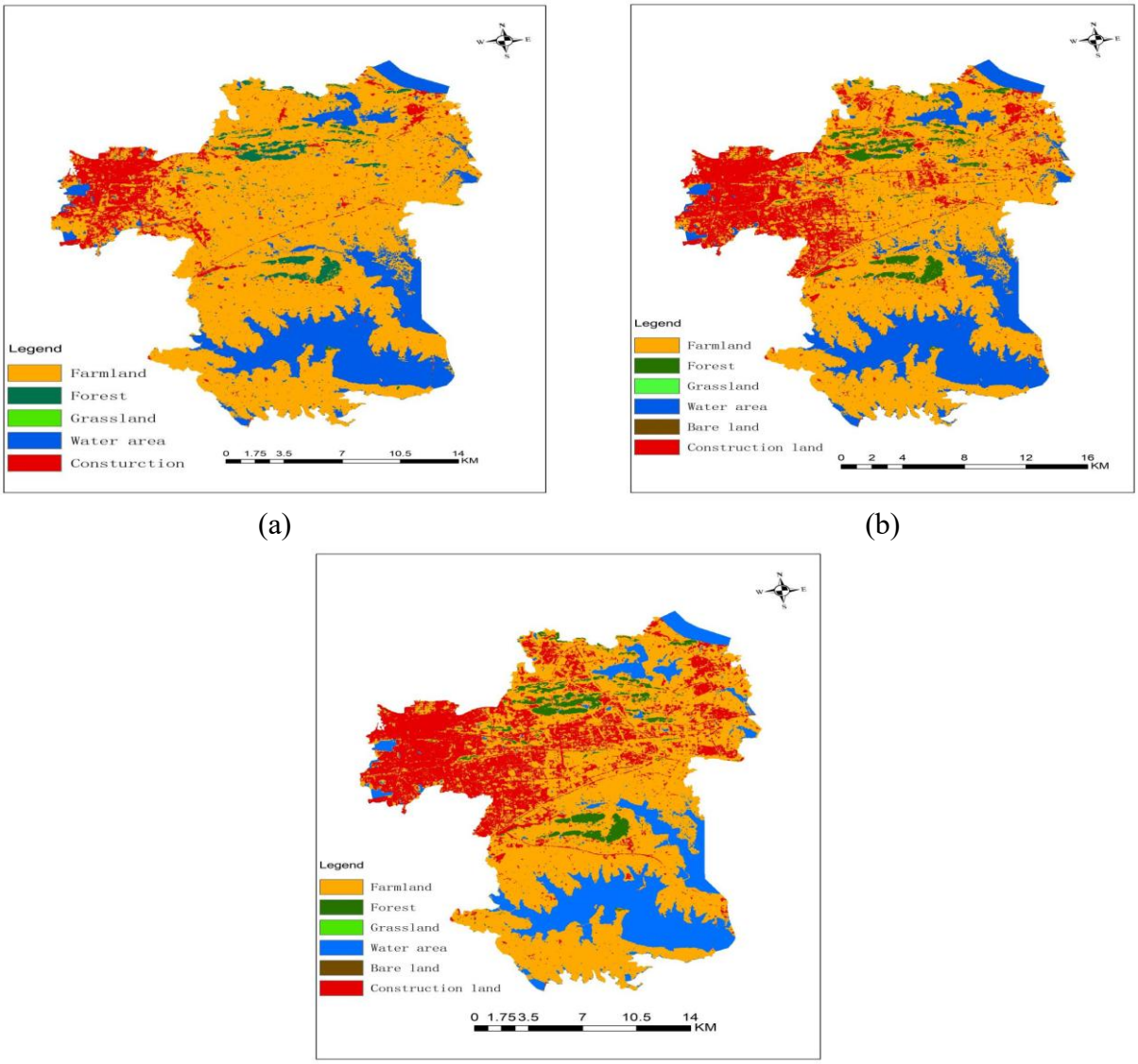


Fig. 3 Land use classification results for (a) 2005, (b) 2015, (c) 2025 (Credit: Original by author).

3.2. Characteristics of NDVI Change

The annual mean NDVI decreased from 0.43 (2005) to 0.38 (2025), a reduction of 11.6%, while the standard deviation increased from 0.18 to 0.24, indicating enhanced spatial heterogeneity (Fig. 4). High-value areas (NDVI > 0.6) were concentrated around East Lake (with the area shrinking from 62.3 km² to 58.9 km²), while low-value areas (NDVI < 0.2) expanded from 38.5 km² to 108.7 km².

At the patch level, green space patches multiplied from 847 to 1,352 while mean patch size dropped from 0.63 km² to 0.38 km²—a clear signal of fragmentation. Zhang et al. found similar trends in their work on urban land use efficiency across the Wuhan metropolitan area. That said, the East Lake core kept its NDVI above 0.55 throughout, so the ecological baseline there stayed relatively intact [12].

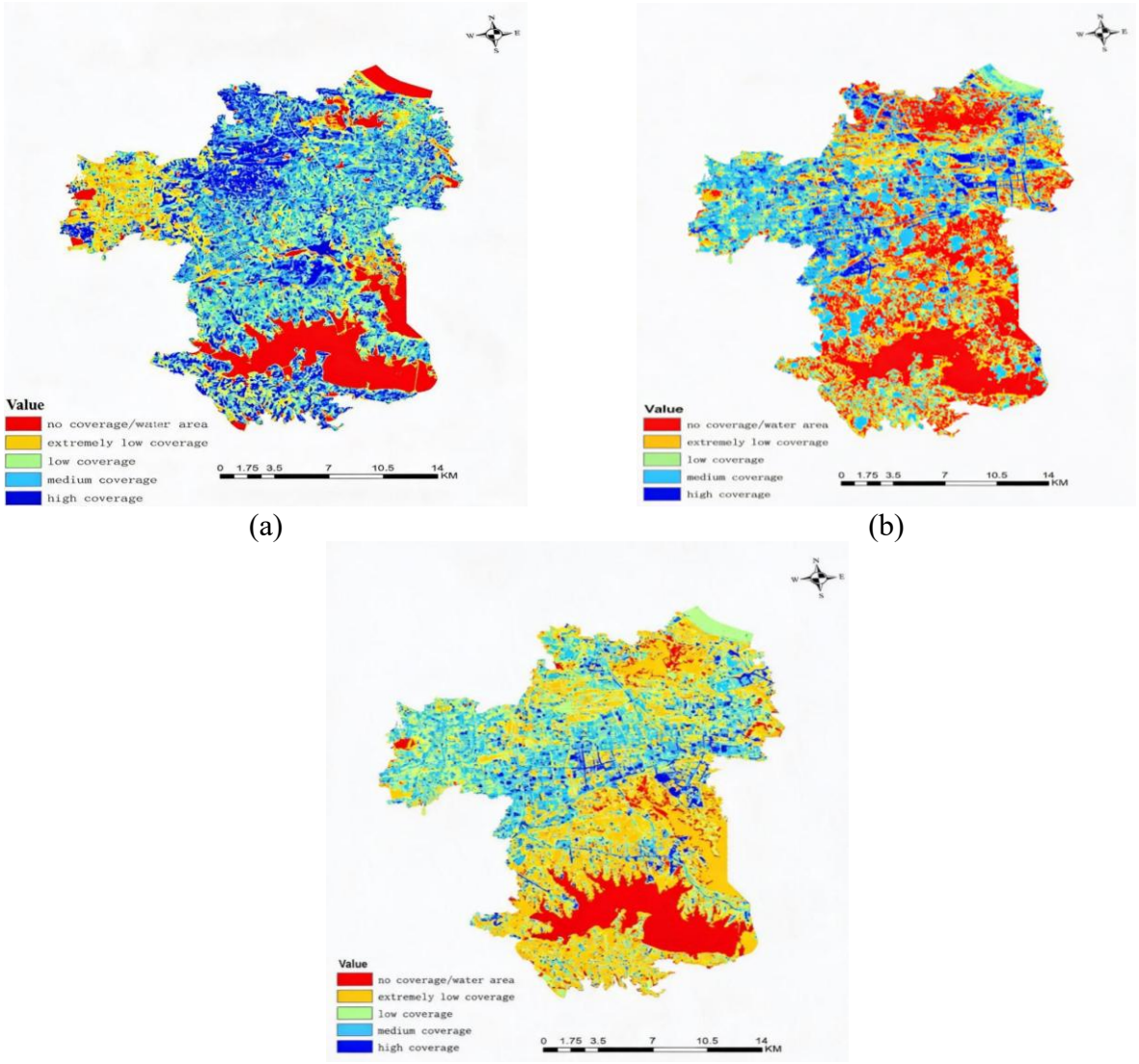


Fig. 4 NDVI maps for (a) 2005, (b) 2015, (c) 2025 (Credit: Original by author).

3.3. Characteristics of Land Surface Temperature Change

LST rose from 28.3°C to 31.5°C over the study period. High-temperature areas (LST > 32°C) ballooned from 45.2 km² to 132.4 km²—a jump of 193%—and urban heat island intensity climbed from 3.6°C to 5.2°C (Fig. 5). Voogt and Oke showed in their foundational review that the urban heat island keeps expanding as construction land grows, with hot spots shifting from scattered points to a connected, areal pattern [13].

Work by Huang and Chen on Wuhan's heat island dynamics also found that the heat island spreads outward as construction land expands [14]. In this study area, East Lake's water temperature held steady at about 22.5°C the whole time, while the temperature gap between the lake and dense built-up zones widened from 4.8°C to 7.3°C—making the lake's cooling effect more pronounced, not less. Hu et al. approached this from a land use conflict angle, reporting that uncontrolled conflict zones in the Wuhan metropolitan area actually dropped from 70.09% to 67.13% between 2000 and 2020, which suggests some overall improvement in land use tensions [15].

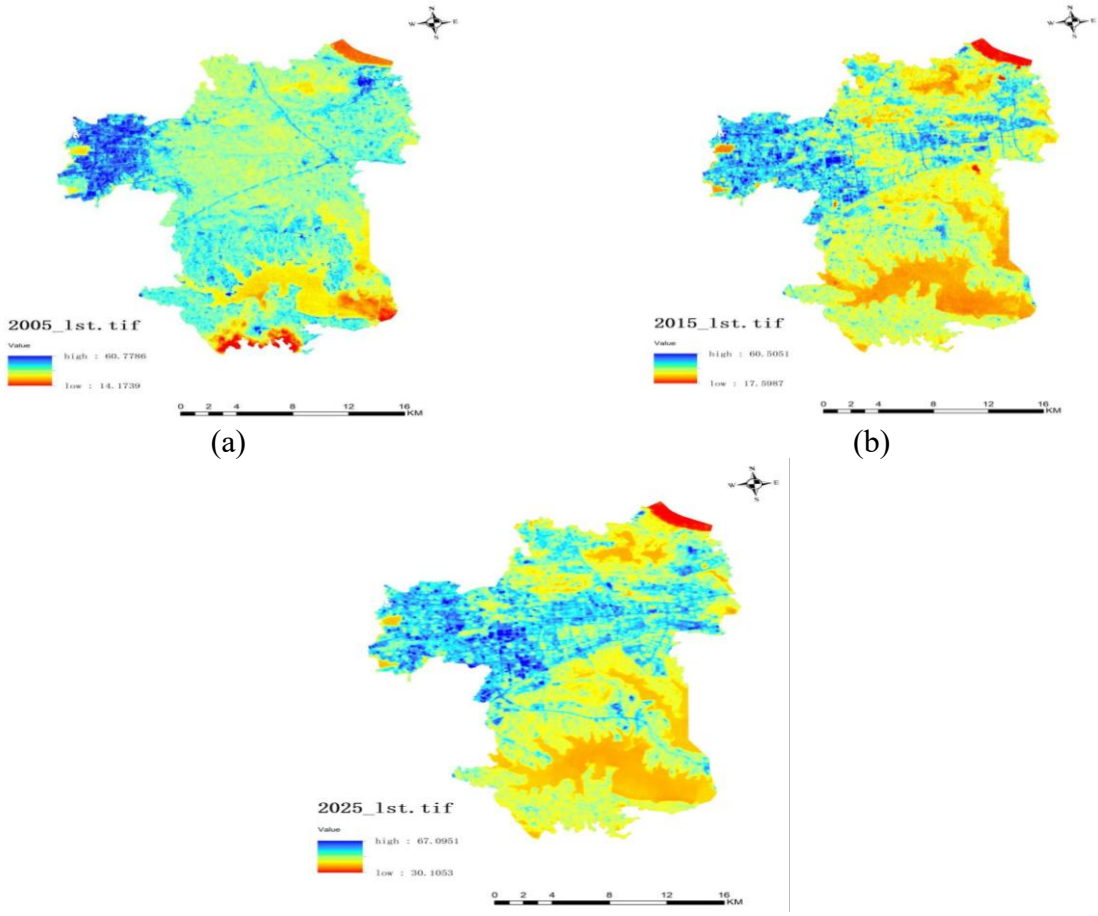


Fig. 5 LST maps for (a) 2005, (b) 2015, (c) 2025 (Credit: Original by author).

3.4. Discussion on the Eco-environmental Responses to Construction Land Expansion

When the land use change, NDVI, and LST results are put together, the coupling is hard to miss. Table 2 (three-period data) shows that construction land proportion has a strong negative correlation with NDVI ($R^2 = 0.91$; each 10-percentage-point increase in construction land proportion corresponds to roughly a 0.06 drop in mean NDVI) and a strong positive correlation with LST ($R^2 = 0.88$; each 10-percentage-point rise brings about a 1.2°C increase in mean LST). Zhang and Wang reported similar coupling features in their analysis of urban expansion and ecological landscape heterogeneity in Wuhan [16]. The impervious surface ratio climbed from 8.42% to 23.50% within the study area, driving both vegetation loss and heat island intensification. Su et al. had already shown that construction land runs hottest among Wuhan's land cover types, followed by cropland, forest, and water [4]. East Lake's role as a large urban lake gave it a steady cooling island effect.

Table 2. Linear regression analysis of construction land proportion with NDVI and LST

Dependent Variable	Regression Equation	R^2	Adjusted R^2	Std. Error	N	F-statistic
NDVI	NDVI = 0.481 − 0.006P	0.91	0.82	0.018	3	10.11
LST (°C)	LST = 27.938 + 0.120P	0.88	0.76	0.97	3	7.33

Table 3. Summary of construction land area, proportion, mean NDVI, and mean LST by year

Year	Construction Land Area (km^2)	Construction Land Proportion (%)	Mean NDVI	Mean LST (°C)
2005	43.61	8.42	0.43	28.3
2015	88.81	17.14	0.40	29.9
2025	121.72	23.50	0.38	31.5

Table 4. Pearson correlation coefficient matrix of construction land proportion, NDVI, and LST

Variable	Construction Land Proportion	NDVI	LST
Construction Land Proportion	1	−0.954	0.938
NDVI	−0.954	1	−0.982
LST	0.938	−0.982	1

The regression and correlation results (Tables 2-4) back up the quantitative coupling story. Rising construction land proportion consistently pushes NDVI down and LST up, with all absolute correlation coefficients topping 0.93-strong linear links among all three. These patterns line up with what Zhang and Wang described for urban expansion and ecological landscape heterogeneity in Wuhan [12].

4. Conclusion

This study examined the spatiotemporal trajectory of construction land expansion and its environmental effects in Wuhan's East Lake High-tech Development Zone, drawing on Landsat imagery and land use data from 2005, 2015, and 2025, plus NDVI and LST indicators. The main findings are as follows.

Firstly, the land use pattern shifted dramatically. Construction land expanded from 43.61 km² in 2005 to 121.72 km² in 2025—a cumulative growth rate of 179.11%—making it by far the most dynamic land use type in the region. Spatially, the built-up area pushed continuously from the urban core eastward and southward, forming larger and more connected patches, while cropland kept retreating under urbanization pressure.

Then, Construction land expansion had a clear impact on vegetation. High-NDVI zones were mostly around East Lake and nearby forested areas, while dense built-up zones consistently showed low NDVI. As construction intensified, low-NDVI patches grew larger and more numerous, and local vegetation patches became visibly fragmented. Even so, East Lake and the green spaces around it held onto relatively high ecological quality and continued to anchor regional ecosystem stability.

Thirdly, Thermal environment changes lined up closely with construction land expansion in space. High-temperature zones kept spreading from 2005 to 2025, expanding outward from the city center. The growth of impervious surfaces from construction land expansion was the main reason behind the regional warming, while water bodies and forested areas showed clear cooling effects. This underscores how important ecological space is for keeping the urban heat island in check.

At last, strong coupling exists among construction land expansion, vegetation cover change, and LST variation. Where construction land increased, vegetation cover consistently dropped, and LST consistently rose. Ecological space, meanwhile, made a positive contribution to regional ecological balance and thermal regulation. The practical implication is straightforward: as urbanization continues, more thought needs to go into how built-up land and ecological space are allocated together, so that land use efficiency and environmental protection can move forward in the same direction rather than at each other's expense.

References

[1] Tong W, Lang F K. Remote sensing monitoring and analysis of land use/cover change in Wuhan City over the past 20 years. Journal of Geomatics, 2022, 46(5): 83-87.

[2] Huang B R, Zhang H Z, Song D J, et al. Driving force analysis of construction land expansion in China's mainland from 2000 to 2010. Acta Ecologica Sinica, 2017, 37(12): 4149-4158.

[3] Chang B R, Li R D. Remote sensing monitoring and spatial differentiation analysis of construction land expansion in Wuhan City. Remote Sensing for Land & Resources, 2022, 29(3): 118-123.

[4] Su Z H, He B Y, Ding C, et al. Analysis of the impact of land use change on the urban heat island in Wuhan based on remote sensing. Journal of Central China Normal University (Natural Science Edition), 2015, 49(1): 139-146.

[5] USGS. Landsat 5 TM, Wuhan area. 2005. https://earthexplorer.usgs.gov

[6] USGS. Landsat 8 OLI/TIRS, Wuhan area. 2015. https://earthexplorer.usgs.gov

[7] USGS. Landsat 8 OLI/TIRS, Wuhan area. 2025. https://earthexplorer.usgs.gov

[8] Resource and Environment Science and Data Center, Chinese Academy of Sciences. National land use raster dataset (30 m). 2020. https://www.resdc.cn

[9] Stewart I D, Oke T R. Local climate zones for urban temperature studies. Bulletin of the American Meteorological Society, 2012, 93(12): 1879-1900.

[10] Yang J X, Gong J, Gao J, et al. Stability and systematic characteristics of land use change in national central cities: A case study of Wuhan City. Resources Science, 2019, 41(4): 701-716.

[11] Huang D, Li R D, Qiu J, et al. Analysis of spatiotemporal land use change and policy driving factors in the Wuhan metropolitan area. Journal of Geo-information Science, 2017, 19(1): 80-90.

[12] Zhang R, Wen L J, Wang N K, et al. Impact of technological innovation on urban land green use efficiency: A case study of 48 districts and counties in the Wuhan metropolitan area. Resources Science, 2023, 45(2): 264-280.

[13] Voogt J A, Oke T R. Thermal remote sensing of urban climates. Remote Sensing of Environment, 2003, 86(3): 370-384.

[14] Huang M H, Chen J J. Spatial and temporal change analysis of urban heat island effect in Wuhan City. ISPRS Archives, 2022, XLIII-B3: 447-452.

[15] Hu Y C, An R, Yang J M, et al. Measurement and driving mechanism of land use conflict based on landscape patterns: A case study of the Wuhan metropolitan area. Research of Soil and Water Conservation, 2024, 31(6): 354-364.

[16] Zhang X S, Wang Y D. Analysis of spatiotemporal heterogeneity of urban expansion and ecological landscape in rapidly urbanizing central China: A case study of Wuhan City. Resources and Environment in the Yangtze Basin, 2023, 32(8): 1583-1593.